Experimental Investigation of Periodically Excited Rotating Composite Rotor Blades

O. Rand*
Technion—Israel Institute of Technology, Haifa, Israel

Experimental procedure for investigating the structural dynamics characteristics of thin-walled composite helicopter rotor blades undergoing periodical excitation during rotation is proposed and demonstrated. The testing setup, which is based on measurements in a vacuum chamber, provides the isolation of the structural dynamics behavior by eliminating the aerodynamic loads and introducing deliberate periodic concentrated loads at the blade's tip. The study presented in this paper includes the testing of thin-walled composite box beams in the nonrotating static case and in the case of periodic loading during rotation at various angular speeds along with comparisons with theoretical predictions. The investigation of the measured composite-related couplings and rotational effects showed some significant nonlinear characteristics.

Introduction

BASED on various levels of approximations, theoretical models capable of analyzing composite beams have been available for more than a decade.[1-12] However, experimental investigations are rare.[13-15] Among the experimental investigations that were aimed toward systematic study of the composite-related coupling effects in thin-walled beams, Ref. 15 represents the state of the art. In this study, a number of graphite/epoxy box beams were fabricated and examined. In addition to their static testing under various tip loads, the blades were excited by piezoelectric elements, which enabled the measurement of natural frequencies and mode shapes.

Experimental investigation of the structural dynamics behavior of helicopter blades usually involves considerable difficulties. Besides the need to be able to apply rotation to the blades and to transmit the measurement readings from the rotating frame to the nonrotating frame, there are difficulties in applying periodic excitation that does not introduce additional uncertainties to the measurements so that the structural dynamics behavior of the blades can be directly measured and subsequently analyzed. The main source of such uncertainties is usually the aerodynamic loads. The prediction of these loads includes a variety of assumptions (such as three-dimensional modeling of a number of lifting surfaces and their wakes, unsteady and viscosity effects, blade interaction, numerical discretization, etc.), which makes it impossible to analytically isolate the structural dynamics behavior.

Within the present investigation, an experimental setup that is capable of providing a direct measurement of the structural dynamics behavior of rotating composite blades has been developed and demonstrated. The blades were built as thin-walled beams having rectangular cross sections. A set of such instrumented blades made of orthotropic laminae with different lay up angles were tested in a vacuum chamber where all of the aerodynamic effects were negligible. The periodic excitation was applied by a tip concentrated force through a special mechanical arrangement.

The experimental setup is described in the following. Then, typical experimental results of static and dynamic testing are presented along with comparisons with predictions based on the theoretical modeling of Ref. 12.

Received July 16, 1990; revision received Jan. 2, 1991; accepted for publication Jan. 31, 1991.

*Faculty of Aerospace Engineering.

Theoretical Background

Theoretical models of thin-walled composite beams are usually based on two main assumptions.[1-12] The first one takes advantage of the blades' high aspect ratio, which enables one to neglect the deformations in the chordwise direction compared with those in the spanwise direction (rigid cross section assumption). The second assumption is based on the small thickness of the cross-sectional walls compared with a typical width (chord), which enables one to assume a state of plane stress throughout the walls. Consequently, the axial stress σ_ξ and the shear stress $\tau_{\xi\eta}$ at each point along the cross-sectional walls may be written as

$$\begin{pmatrix}\sigma_\xi\\ \tau_{\xi\eta}\end{pmatrix}=\begin{bmatrix}C_{11} & C_{16}\\ C_{16} & C_{66}\end{bmatrix}\begin{pmatrix}\epsilon_\xi\\ \gamma_{\xi\eta}\end{pmatrix} \tag{1}$$

where C_{11}, C_{66}, C_{16} are elastic moduli and ϵ_ξ, $\gamma_{\xi\eta}$ are axial and shear strains, respectively. Usually, in the case of multilayered skin, the elastic moduli are taken to be the equivalent moduli that are obtained by averaging these quantities according to the modulus and thickness of each lamina. Thus, compared with isotropic blades, the second assumption mentioned above leads to an additional elastic modulus C_{16} that couples shear strain with axial stress and axial strain with shear stress.

As shown by Eq. (1), proper prediction of the shear strain distribution $\gamma_{\xi\eta}$ is essential in the case of nonvanishing coupling since it plays a role in the determination of both axial and shear stresses. As a result, the ability to predict this shear strain accurately, which is a function of the ability to provide detailed out-of-plane warping distribution, is one of the important characteristics of the theoretical models. Thus, experimental data regarding the behavior of ϵ_ξ and $\gamma_{\xi\eta}$, which are proposed by the present study, provide both better insight into the problem and may help in assessments of the theoretical models. It should be mentioned that the theoretical predictions of Ref. 12, which will be used in what follows, are also based on the above assumption of constant strain throughout the wall thickness [see Eq. (1)]. However, for the wall thickness of the cross section under discussion in the present paper, this assumption is expected to have only a minor effect.

Experimental Setup

Vacuum Chamber

A schematic view of the experimental setup is presented in Figs. 1a and 1b. As shown, a single blade and a countermass are rotated in a cylindrical vacuum chamber by an external variable-speed electric motor. The blade is clamped to the rotation axis at an adjustable distance from it. A load cell is

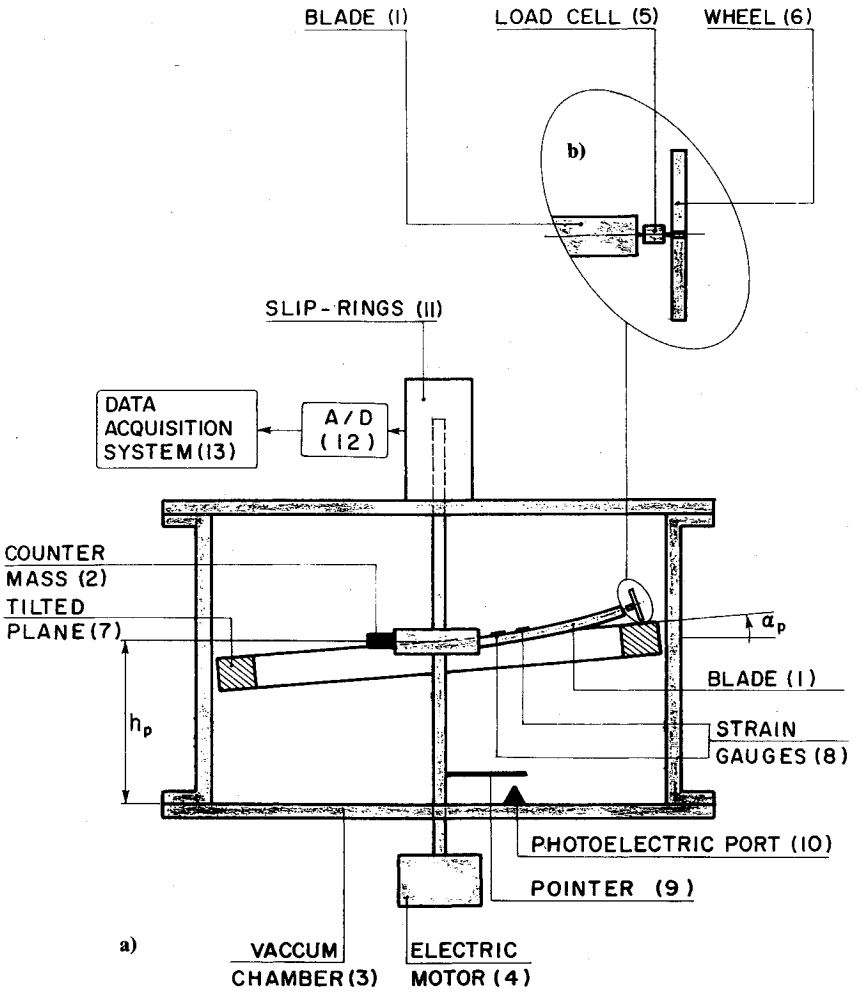

Fig. 1 Schematic view of the experimental setup.

connected to the blade at its tip and to a small wheel that moves along the circumference of a tilted ring plane. The tilt angle of this plane α_p and its height h_p may be adjusted. Consequently, the blade tip is forced to trail the plane's circumference, which creates a 1/revolution excitation. For the sake of convenience, the azimuth angle $\psi = 0$ has been chosen at the location where the tilted plane reaches its maximum height and the azimuth angle $\psi = 180$ deg refers to the minimum height position. Thus, the blade flatwise tip displacement may be written as

$$w_t = w_o + w_c \cdot \cos\psi \tag{2}$$

where w_o and w_c are adjustable.

During a test, the load cell measures the time-dependent force acting on the blade's tip in the vertical (flatwise) direction and in the horizontal (edgewise) direction (see details in Fig. 1b), whereas the mechanical arrangement ensures no torsional moment or torsional constraint at the tip. Strain gauges are located at various locations over the blade.

The blade's azimuthal position is determined by an additional signal that arises from a reference pointer that is connected to the rotating system and passes over a photoelectric port once in each revolution.

All strain gauges and load-cell readings and the pointer signal are transmitted to the nonrotating frame by a system of slip rings. These readings are then passed through an analog/digital converter and fed into a computerized data acquisition system.

Thus, knowing the loads acting at the blade's tip (which are measured by the load cell) provides complete experimental data where the tested blade is submitted to known tip periodic loads and performs given tip flatwise deformations while the time-dependent strains over its walls are also measured.

Composite Blades

In the present study, thin-walled uniform composite blades having a rectangular cross section and made of P109/glass orthotropic laminae were tested. A scheme of a typical blade is shown in Figs. 2a–2c. To clarify the following discussion, two reference systems of coordinates (x,y,z) and (ξ,η,ζ) are also shown in this figure. The origin of the (x,y,z) system is located at the middle of the blade's cross section at its root, the x-coordinate line connects all of the cross-section centers, and the x-y plane is parallel to the blade's horizontal walls. The local system of coordinates (ξ,η,ζ) is located at each point along the cross-sectional walls, ξ is parallel to x, and η is tangent to the local contour.

All blades were made of four identical orthotropic (cloth) laminae. Fabrication was based on room temperature hand lay up using a mold and cured under pressure according to the material processing specifications. Overlapping of the plies was limited to a small area at the cross-sectional corners. For each blade, the angle θ between the principal axis of the laminae and the x-coordinate line (see Fig. 2b) was different but constant along the entire contour. This case is usually referred to as the antisymmetric case. Three different blades were tested: blade 1 where $\theta = 0$, blade 2 where $\theta = 22$ deg, and blade 3 where $\theta = 45$ deg. The weights of the blades were practically identical (0.08 kg/m).

As stated earlier, the blades are equipped with strain gauges. There are four strain rosettes over each blade—two on the upper horizontal wall and two on the lower horizontal wall. This enables the measurement of the normal strains ϵ_ξ and the

evaluation of the shear strain $\gamma_{\xi\eta}$ at each point. Following the notation of Fig. 2c, the blade dimensions and the gauge locations are the following: $L = 0.285$ m, $b = 0.028$ m, $h = 0.007$ m, $t = 0.0008$ m, $r_1 = 0.01$ m, and $r_2 = 0.155$ m.

Load Cell

The load cell has been designed to give separate readings of the vertical (flatwise) force and the horizontal (edgewise) force. By using the output readings of a number of strain gauges located on the load cell, it became possible to combine these readings in such a way that will compensate for possible induced measurement noises.

It should be noted that there are some additional small loads acting on the blade due to the mass of the joint used to connect the load cell to the blade and due to small gyroscopic effects that are created by the wheel's spinning during rotation. However, these are purely dynamic effects that are fully predictable since all of the involved parameters are known including the tip flatwise motion. Calculations have shown that these effects are negligible, although it is possible to take them into account as part of the tip loads.

Test Procedure

The following are the main stages of a typical test procedure:

1) The load cell and strain gauges are calibrated.

2) The height h_p and the tilt angle of the plane α_p are set to their required values.

3) The vacuum pump is turned on to create sufficient vacuum level (usually 650 mm Hg).

4) The electric motor is turned on and set to give the required rotational speed (up to 1000 rpm).

5) Load-cell and strain-gauge readings are taken (at the rate of 2000 Hz) and stored digitally in the data acquisition system.

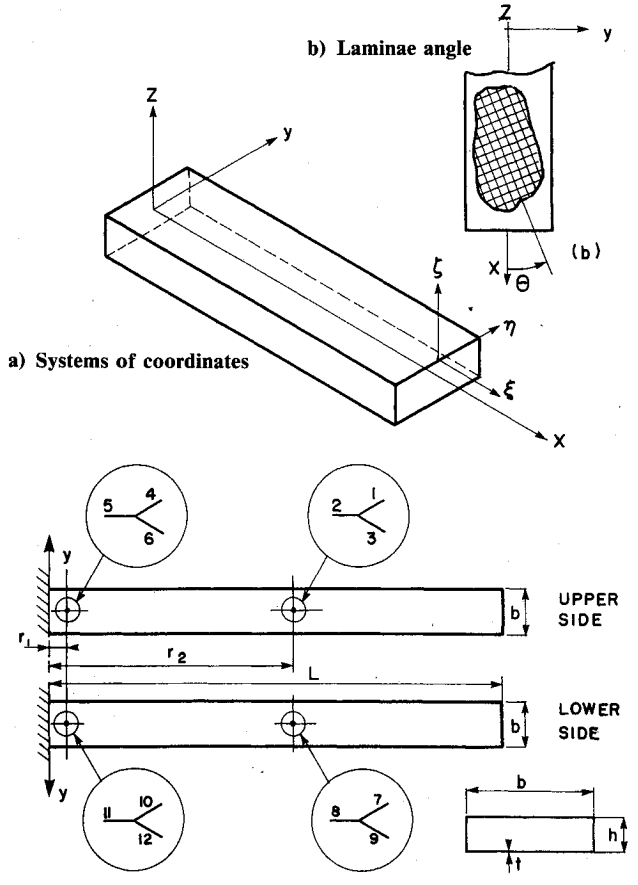

Fig. 2 Structure and dimensions of the blades.

Results and Discussion

Properties of the Blades

Preceding the study of the behavior of the blades under dynamic loads, the structural properties of the blades were estimated using experiment/theory correlation study for simple static cases that will be described in this section. Typically, 7–10 specimens were fabricated for each lamination angle. The results presented in what follows are of one blade from each group that exhibits averaged characteristics of that group. The spreading of the experimental results of this study may also provide an indication regarding the quality of the tested specimens. As mentioned earlier, the blades differ only by their laminae angle θ relative to the x directions (see Fig. 2b). Therefore, in order to measure the effective skin properties, it is convenient to use the uncoupled blade ($\theta = 0$) as a reference where only two nonvanishing elastic moduli have to be measured. This enables the prediction of the elastic moduli of blades having nonvanishing composite couplings.

The uncoupled blade (blade 1) has been tested under successive tip flatwise forces and tip torsional moments. Figure 3a presents the strain at gauges 2, 8, 5, and 11 (see also Fig. 2c) as a function of the flatwise tip force. In addition, the strain in the η direction, ϵ_η, which has been calculated by the three measurements of the strain rosette, is shown in Fig. 3b as a function of the axial strain ϵ_ξ for various points along the blade.

The full lines in Figs. 3a and 3b are the theoretical prediction of this case that were obtained for blade 1 by assuming that the effective extension elastic modulus C_{11} and the Poisson's ratio ν_{12} are 1.53×10^{10} N/m^2 and 0.14, respectively.

The uncoupled blade 1 enables also a simple measurement of the shear modulus C_{66} by means of measuring the shear strains along the blade that are created by a tip moment in the x direction. The results for this case are presented in Fig. 4. The corresponding theoretical prediction, which is presented by a full line in Fig. 4, yields good correlation with the experimental data provided that $C_{66} = 0.25 \times 10^{10}$ N/m^2.

Transformation of the previously mentioned properties of blade 1 to the case of nonvanishing laminae angles yields the predicted properties of blades 2 and 3. Table 1 summarizes these results. As shown, blade 1 is uncoupled with $C_{66}/C_{11} = 0.16$, blade 2 has composite coupling, and blade 3 is a

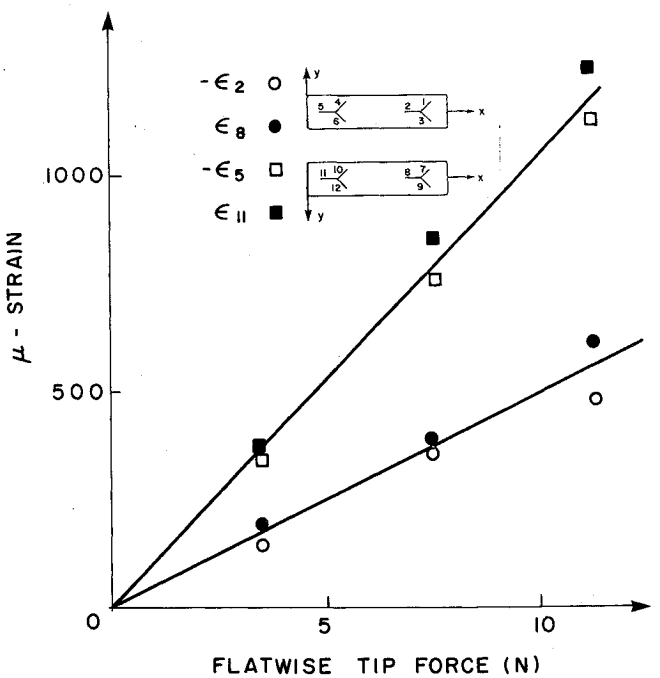

Fig. 3a Axial strain as function of the tip flatwise force (uncoupled blade).

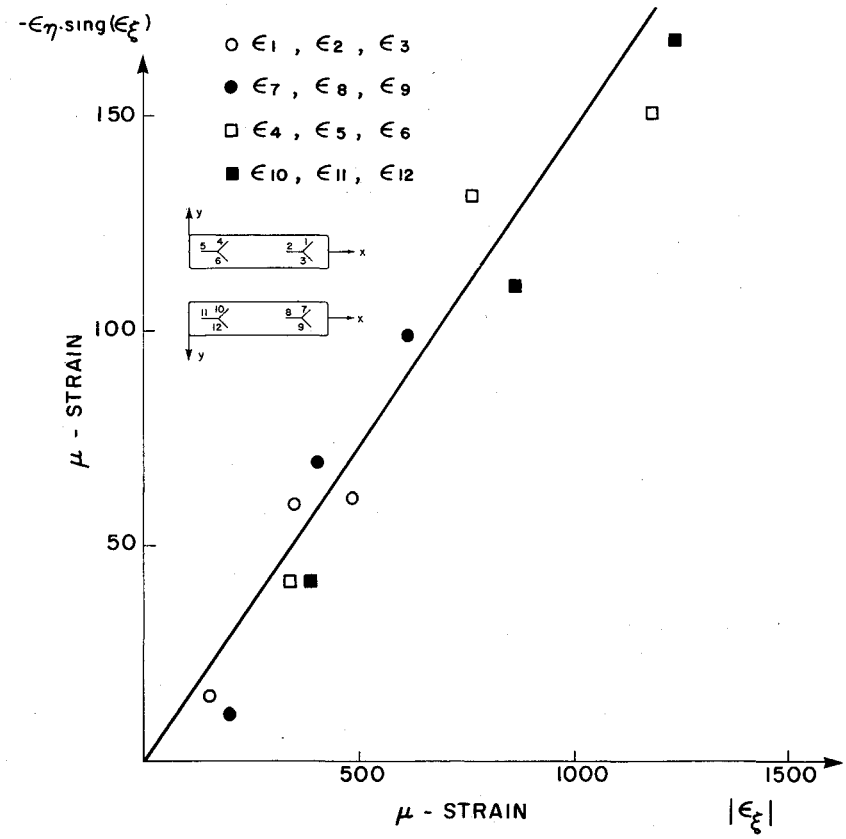

Fig. 3b Chordwise strain as function of the axial strain (uncoupled blade).

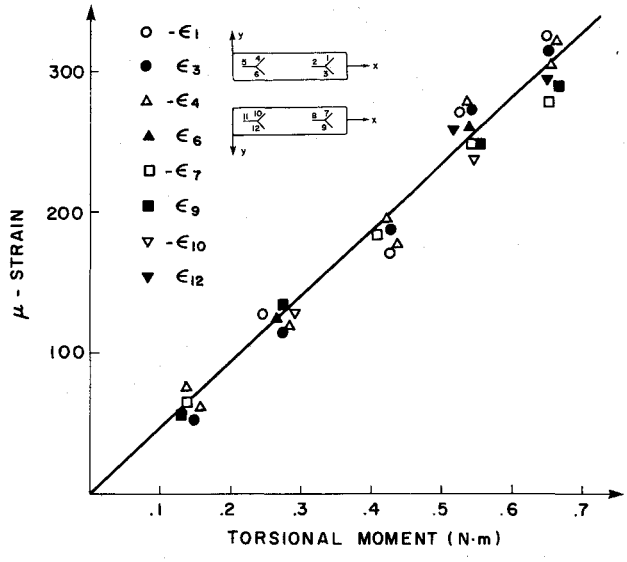

Fig. 4 Strains as functions of tip torsional moment (uncoupled blade).

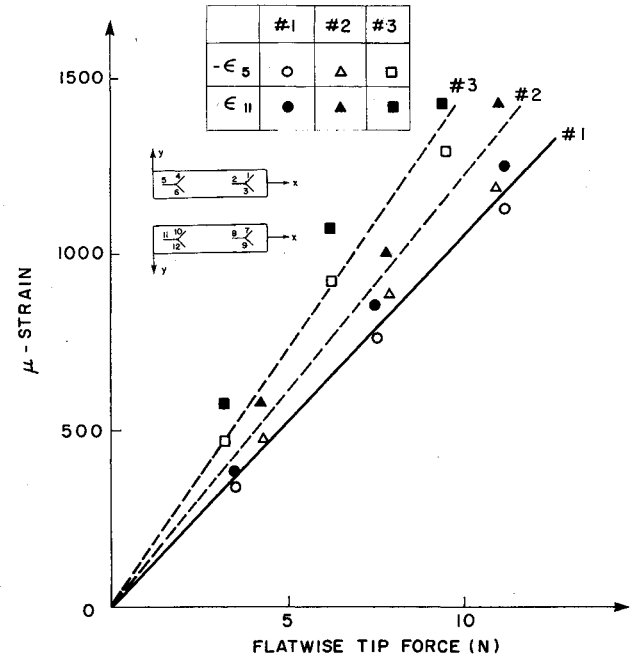

Fig. 5 Axial strains as functions of the flatwise tip force.

quasi-isotropic blade with relatively high shear modulus—$C_{66}/C_{11} = 0.59$.

Partial validation of the calculated properties of blades 2 and 3 are presented in Fig. 5. In this figure, the longitudinal strains at gauges 5 and 11 are presented as a function of the flatwise tip force for all blades. The dashed lines represent the theoretical predictions that were carried out for blades 2 and 3 according to the tabulated values of the elastic moduli. The correlations presented in this figure confirm the reduction in the flatwise stiffness with increasing values of θ, as shown by Table 1.

Static Behavior

As a first step toward the investigation of the structural dynamics behavior of the blades, the blades were tested statically. This part of the experiment includes the measurement of the main features of antisymmetric blades, namely, the extension-torsion coupling and the bending-shear coupling. As shown in Ref. 12, these couplings are the result of the nonvanishing elastic modulus C_{16} that connects normal stresses to shear strain and shear stress to normal strain [see also Eq. (1)]. In the following tests, the blades were clamped at their root by

placing them in a rigid frame. However, out-of-plane warping was not completely restrained.

Extension-Torsion Coupling

To measure the extension-torsion coupling mechanism, the blades were subjected to a tip tension force varying between 0 and 80 N. The force was applied by a weight that was connected to the blade's tip in a way that no twist, bending slopes, or warping constraints were induced. The tip rotation angle has been measured using a thin stick of negligible weight, which was connected as a pointer to the blades tip and amplified the readings over a large screen. The results of this test for blade 2 are presented in Fig. 6. As shown, the tip twist grows nonlinearly with the tip load. The linear theoretical calculations in this case predict a slope that is smaller than the experimental one even for the low loads region. Accordingly, nonlinear modeling of this case seems to be inevitable.

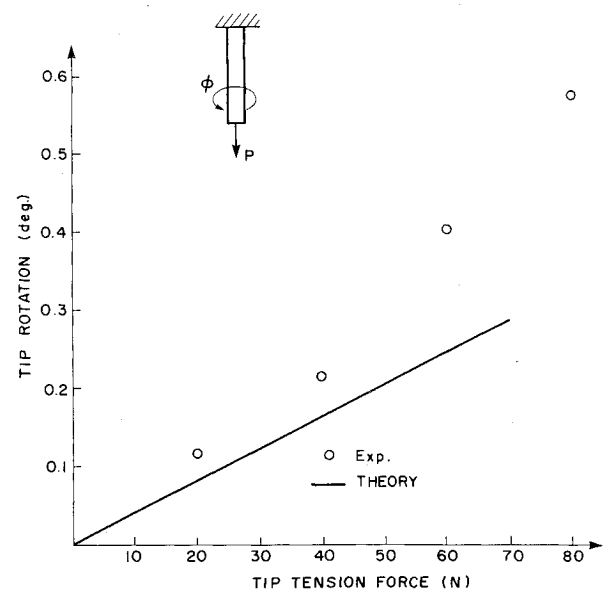

Fig. 6 Theory/experiment correlation of the tip rotation as function of the tip tension force (coupled blade).

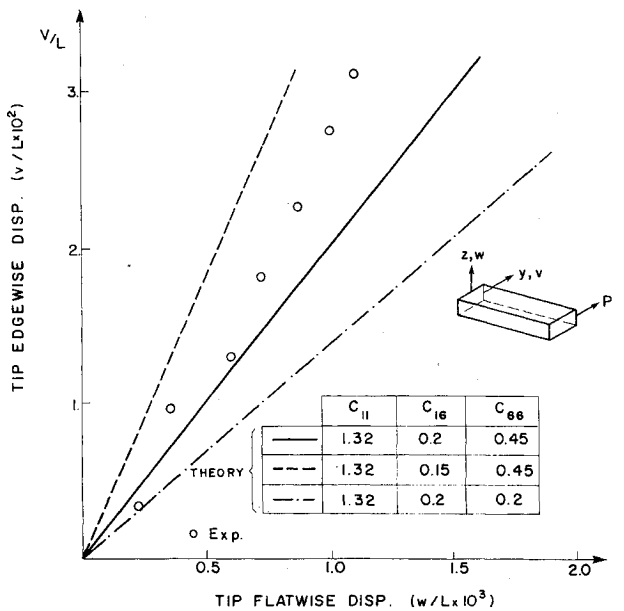

Fig. 7 Tip edgewise displacement vs tip flatwise displacement due to tip edgewise force (coupled blade).

Table 1 Elastic moduli of the blades ($\times 10^{-10}$ N/m^2)

Blade	C_{11}	C_{16}	C_{66}
1	1.53	0.0	0.25
2	1.32	0.20	0.45
3	1.12	0.0	0.66

Bending-Shear Coupling

Static study of the bending-shear coupling has also been carried out for blade 2. In this case, the clamped blade was subjected to a series of increasing tip loads in the y direction. As in the previous case, an amplification technique was used to measure the resulting tip deflections in the y and z directions. The results are presented in Fig. 7 along with the theoretical predictions for this case. Compared with the previous correlation, the agreement in this case is better. As shown, relatively small values of flatwise displacements are created by the bending in the edgewise direction. (Note that the horizontal and vertical axes are scaled differently.) It should be mentioned that, according to the theoretical predictions of Ref. 12, it is expected that the resulting edgewise displacements due to flatwise bending would be much smaller. To demonstrate the sensitivity of this coupling effect to the elastic moduli values, two additional calculations of a blade with slightly different properties are also given in Fig. 7. Note that both increasing the C_{16} modulus and decreasing the C_{66} modulus tend to increase the bending-shear coupling effect. Detailed insight and explanation of these couplings may be found in Ref. 12.

Dynamic Behavior

Free Vibrations

Prior to the study of the response of the blades to periodic loads, the blades were tested under the action of a vibrator that generated vibratory point load in the flatwise direction at the blades' roots. The nonrotating blades were cantilevered during this test. Examination of the gauge's response in this case enables simple detection of the free vibration frequency. The first mode frequency is presented in Fig. 8 along with the theoretical predictions. Note that the C_{11} elastic modulus predominates the flatwise vibratory motion in this case. As shown, the theoretical calculations are consistently high; however, the general decrease in the natural frequency with respect to C_{11} is well predicted. The discrepancy presented in Fig. 8 seems to originate from the imperfect clamping conditions at the root and, in particular, from the absence of warping constraints. To enable comparison with full-scale blades, theoretical prediction of Southwell's plot for the natural frequencies was performed. Denoting the natural and the rotational frequencies by ω and Ω, respectively, the theoretical predictions enable the following approximations:

$$\omega^2 = K_1 + K_2\Omega^2 \tag{3}$$

If ω and Ω are given in cycles per second, the values of K_1 are 4624, 3969, and 3364, and the values of K_2 are 3.48, 4.59, and 5.89 for blades 1, 2, and 3, respectively.

Periodic Response

Typical results of the study of the behavior of the blades under periodic excitation are presented in this section. In the following tests, the blades were clamped at a distance of 0.03 m from the rotation axis. In some of these time-dependent results, two lines will be presented for each case: a noisy (full) line, which represents the actual measurement, and a smooth (dashed) line, which represents the result of filtering the high harmonics. Although each test is based on a number of revolutions (usually 10-20), only the behavior of a single typical revolution is presented. Comparison of various revolutions of the same test showed extremely high correlation and were practically identical.

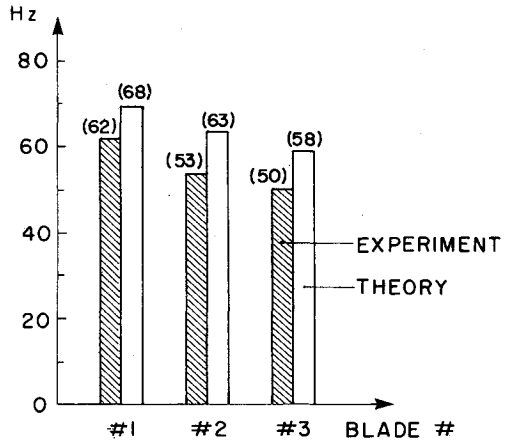

Fig. 8 Theory/experiment correlation of the first mode's frequency.

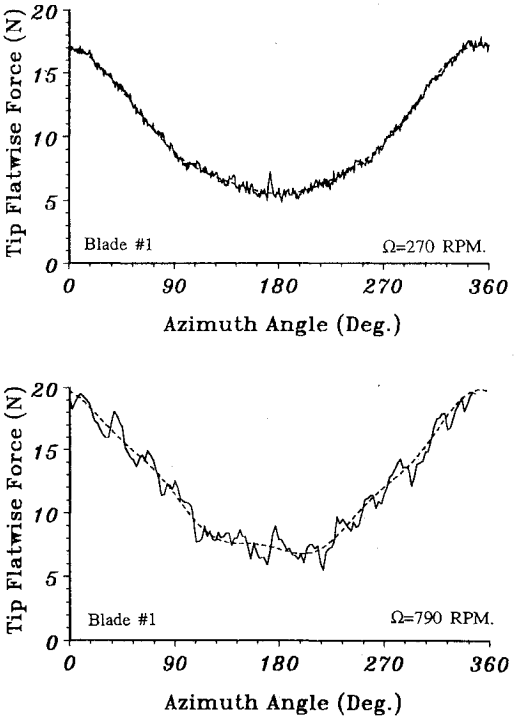

Fig. 9 Tip flatwise force for two different angular velocities (uncoupled blade).

The load-cell readings for blade 1 are dealt with first. In Figs. 9a and 9b, the flatwise load that was measured by the load cell is presented for two different angular velocities. As shown, the vertical force is increasing with speed since the plane tilt angle was kept constant throughout these tests and the centrifugal force component in the flatwise direction had to be compensated. Compared with metal blades, the stiffness/weight ratio of composite blades is high and, therefore, the differences in the flatwise force between these two angular speeds is relatively small. By comparing Figs. 9a and 9b, dynamic effects in the blade's behavior can be recognized. At low angular velocity (Fig. 9a), the vertical force tracks the blade tip flatwise displacement and, therefore, reaches its maximum and minimum values very close to the azimuth angles of 0 and 180 deg, respectively [which are also the maximum and minimum locations of the flatwise tip displacement—see Eq. (2)]. At high rotational speed, it can be seen from Fig. 9b that, after decreasing in the $0<\psi<90$-deg region, the tip load decreasing rate is reduced around $\psi = 100$ deg before the minimum tip load is reached (at $\psi \cong 200$ deg). This is a consequence of the blade's flatwise inertia, which acts downward at that region.

The time-dependent edgewise force that is transferred to the blade through the load cell is shown in Figs. 10a and 10b. Compared with the flatwise excitation, the edgewise load is relatively small and hardly varies with the angular speed.

The strain-gauge measurements are dealt with next. The axial strains over the upper and lower horizontal walls of blade 1 are presented in Fig. 11a. As shown, these strains perform a substantial 1/revolution motion with relatively

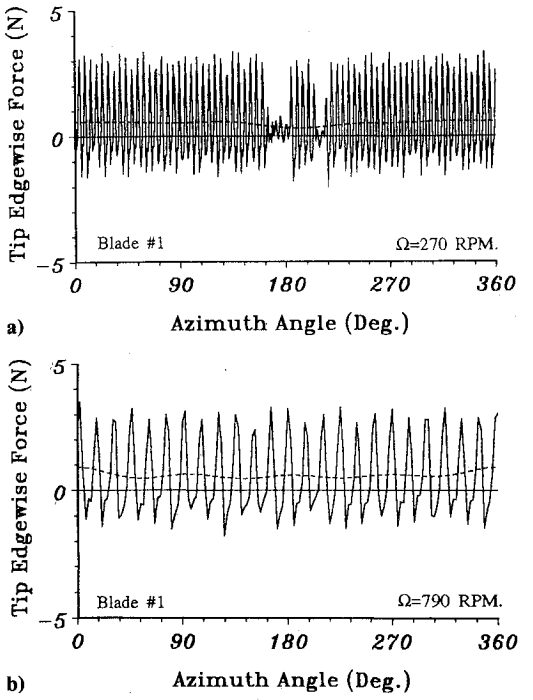

Fig. 10 Tip edgewise force for two different angular velocities (uncoupled blade).

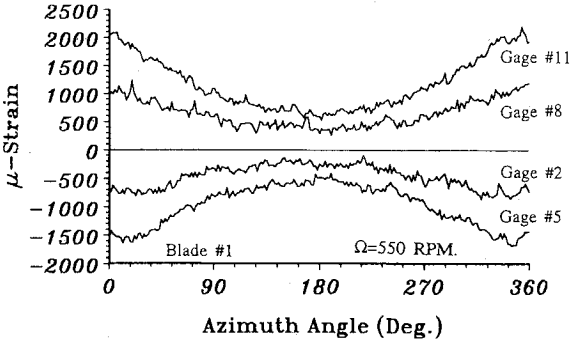

Fig. 11a Axial strains over the upper and lower horizontal walls (uncoupled blade).

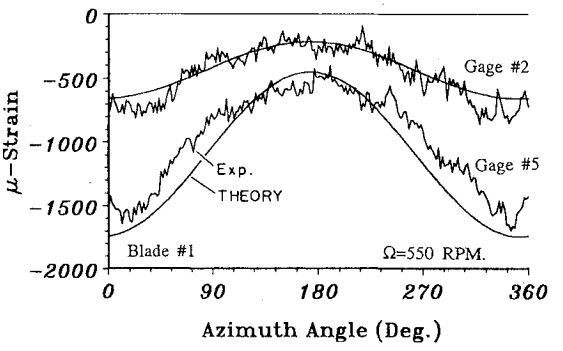

Fig. 11b Theory/experiment correlation of the axial strains over the upper horizontal wall (uncoupled blade).

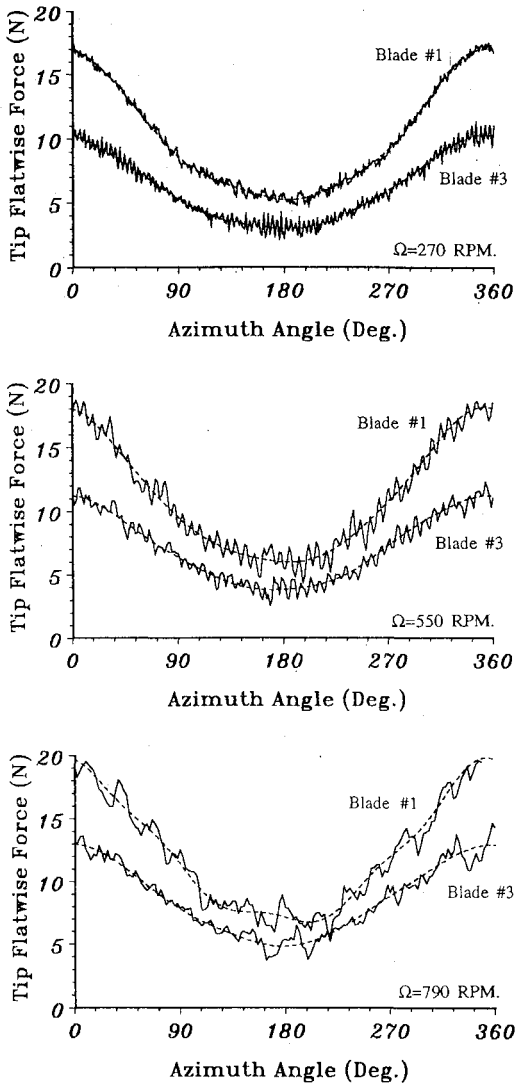

Fig. 12 Tip flatwise force for three angular velocities (uncoupled blades).

small amplitude higher harmonic components. It is evident that, unlike the case of nonrotating bending, the behavior is not symmetric (i.e., the absolute values of the readings of gauge 2 are not identical to those of gauge 8 and the same is true for gauge 5 and gauge 11). This is due to the additional extension strain that is caused by the rotation. Theoretical predictions that were based on the first harmonic of the tip force are presented in Fig. 11b for gauges 2 and 5.

Comparisons between the uncoupled blades (blades 1 and 3) at constant tip deflection (both magnitude and first harmonic) are presented in Figs. 12a–12c and 13a–13c for three speeds. It is shown that, due to the different stiffnesses, there are notable differences in the flatwise tip force (Figs. 12a–12c). Examination of the extension strain at gauge 11 for these blades (Figs. 13a–13c) shows that, as expected, for low speed the strains are similar. However, as speed increases, differences start to appear due to the stiffnesses differences and the nonlinear influence of the rotational effects. These effects are usually negligible in static cases and their analytical prediction requires the introduction of nonlinear geometrical terms as well.

The axial strain in gauge 11 of blade 2 exhibits similar behavior. Figure 14 presents a comparison of this strain in blade 2 with the theoretical predictions. As shown, the predicted amplitude is slightly higher, which may result from constraints in the root region that are not fully modeled by the theory.

The extension-torsion coupling effect in antisymmetric composite blades that was statically demonstrated earlier using a tip tension force is one of the main features of rotating composite helicopter blades. To demonstrate this effect, the strains in gauges 7, 8, and 9 of blade 2 are presented in Fig. 15a. Using the filtered results of these measurements, the shear strain $\gamma_{\xi\eta}$ has been calculated. Then, with the aid of Eq. (1), the axial and shear stresses σ_ξ and $\tau_{\xi\eta}$ were determined. The calculated results are presented in Fig. 15b. As shown, the shear strain is negative (which corresponds to twist in the positive x direction—see Fig. 2a). However, the shear stress is

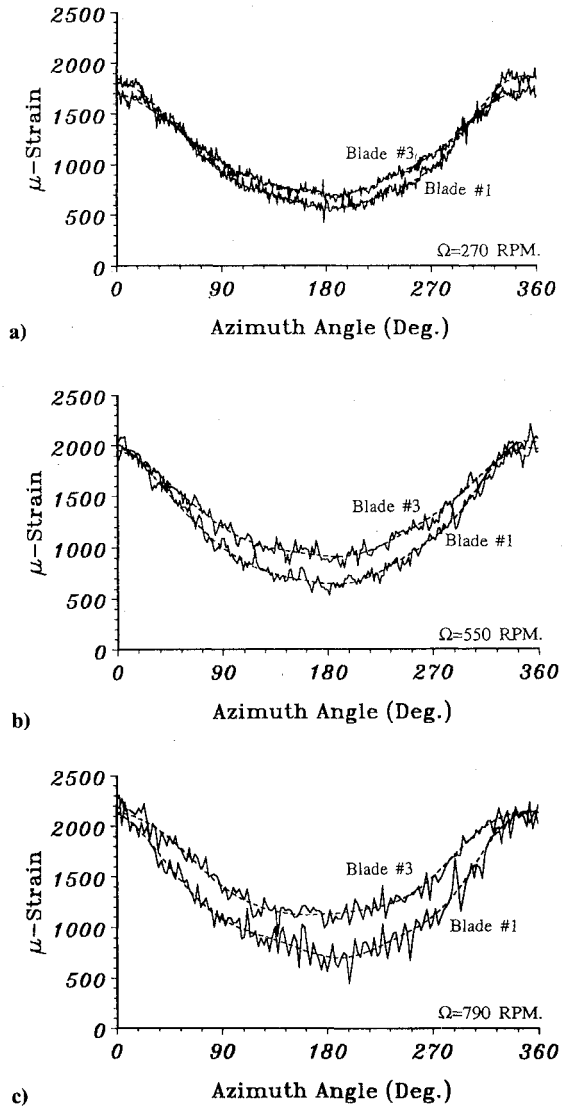

Fig. 13 Axial strains at the lower horizontal wall for three angular velocities (uncoupled blades).

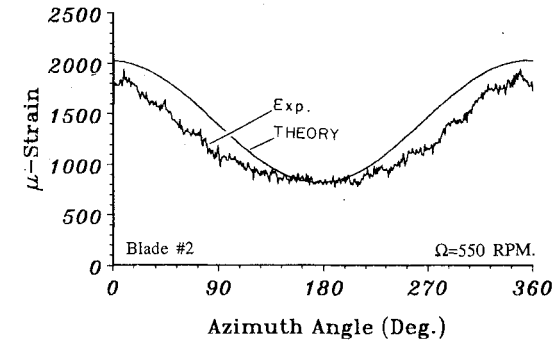

Fig. 14 Theory/experiment correlation of the axial strain over the lower horizontal wall (coupled blade).

practically zero. This is due to the opposite contributions of the terms $C_{16} \cdot \epsilon_\xi$ and $C_{66} \cdot \tau_{\xi\eta}$ [see Eq. (2)], which are shown by dashed lines in Fig. 15b. This interesting consequence is expected since no torsional moment is imposed and the resulting shear strain is the outcome of twist that has been created only by the composite related coupling effects.

Comparison of the shear strain variation with the corresponding theoretical prediction is presented in Fig. 16. Although relatively high discrepancies exist, similar trends may be observed. It should be mentioned that, since the shear strains are small, their prediction in cases where they are coupled with large axial strains is difficult.

A similar picture to that of Figs. 15a and 15b is observed at the inboard station of blade 2 (gauges 10, 11, and 12), as shown in Figs. 17a and 17b. Note that the axial stress is much higher at this point; however, the shear strain (which represents the twist) is similar to the previous case.

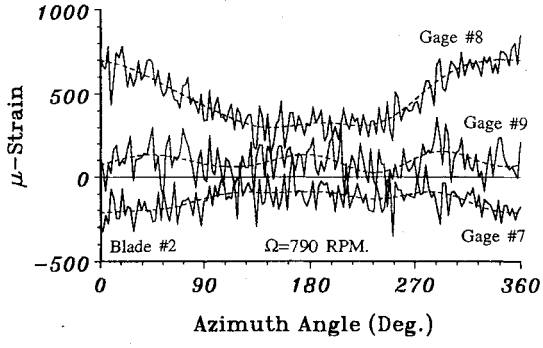

Fig. 15a Strains at the outboard station over the lower horizontal walls (coupled blade).

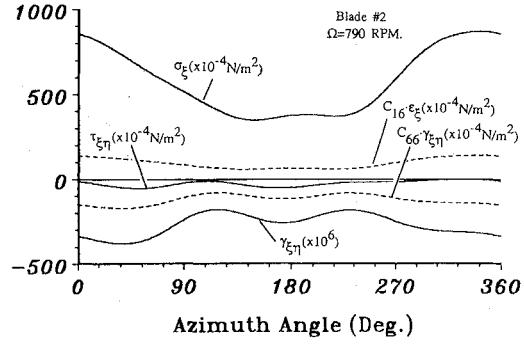

Fig. 15b Shear strain and stresses at the outboard station over the lower horizontal wall (coupled blade).

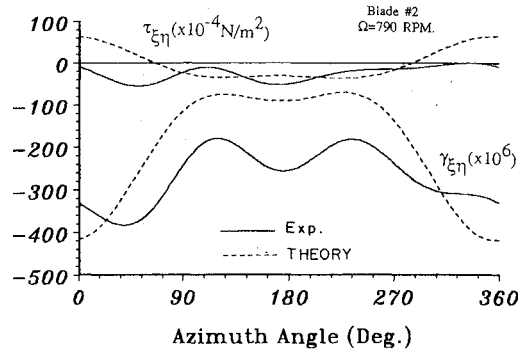

Fig. 16 Theory/experiment correlation of the shear strain and shear stress at the lower horizontal wall (coupled blade).

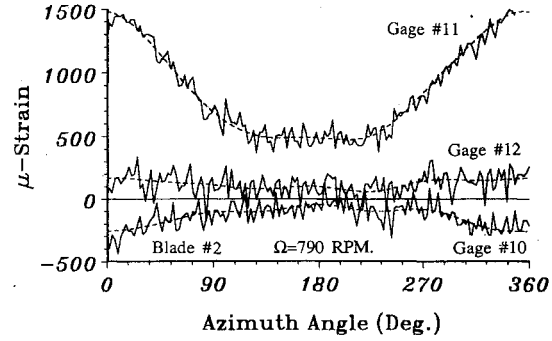

Fig. 17a Strains at the inboard station over the lower horizontal walls (coupled blade).

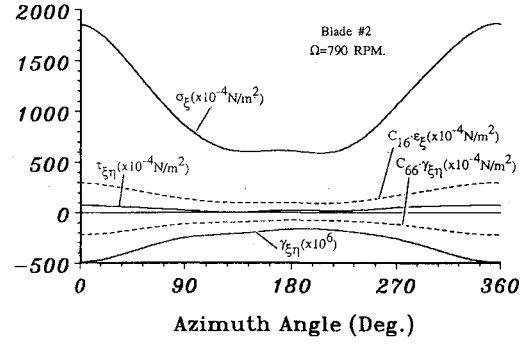

Fig. 17b Shear strain and stresses at the inboard station over the lower horizontal wall (coupled blade).

Concluding Remarks

An experimental study of periodically excited thin-walled composite blades has been presented. The experimental setup is based on a unique arrangement that allows the introduction and measurement of periodic tip loads forced upon the blades while the resulting strains at selected locations are also measured.

By isolating the structural dynamics behavior, this testing method may serve as a basic tool during the development of new blades. Moreover, by eliminating uncertainties concerning the aerodynamic loads, it supplies ideal results for correlation of structural dynamics computer codes and enables the study of fine structural dynamics effects.

The potential of the proposed technique to serve as a testing facility for studying the structural dynamics behavior of various helicopter blades has been demonstrated by examination of different blades in various angular speeds.

Comparisons with analytical predictions showed general reasonable agreement and pointed out a few regions where improvements in prediction capability is needed.

The following are the most important characteristics observed by the present investigation:

1) The extension-torsion coupling exhibits nonlinear behavior even for relatively low and static tension loads.

2) The bending-shear coupling may be reasonably determined by linear theory.

3) The nonlinear effects of shear modulus/axial modulus ratio that are usually negligible in static cases become significant during rotation and should be taken into account in theoretical predictions.

4) It has been confirmed that, compared with typical isotropic (metal) blades, the effective rotational stiffness is relatively small in composite blades due to their high stiffness/weight ratio.

References

[1]Mansfield, W. H., and Sobey, A. J., "The Fiber Composite Helicopter Blade, Part 1: Stiffness Properties, Part 2: Prospects for Aeroelastic Tailoring," *Aeronautical Quarterly,* Vol. 30, May 1979, pp. 413–449.

[2]Rehfield, L. W., "Design Analysis Methodology for Composite Rotor Blades," *Proceedings of the Seventh Conference on Fibrous Composites in Structural Design,* AFWAL-TW-85-3094, U.S. Air Force, V(a)-1-V(a)-144, 1985.

[3]Wörndle, R., "Calculation of the Cross Section Properties and the Shear Stress of Composite Rotor Blades," *Vertica,* Vol. 6, 1982, pp. 111–129.

[4]Giavotto, V., Borri, M., Mantegazza, M., Ghiringhelli, G., Carmashi, V., Maffioli, G. C., and Mussi, F., "Anisotropic Beam Theory and Applications," *Computer and Structures,* Vol. 16, 1983, pp. 403–413.

[5]Hong, C. H., and Chopra, I., "Aeroelastic Stability Analysis of a Composite Rotor Blade," *Journal of the American Helicopter Society,* Vol. 26, No. 2, 1985, pp. 57–67.

[6]Hong, C. H., and Chopra, I., "Aeroelastic Stability of a Composite Bearingless Rotor Blade," *Journal of the American Helicopter Society,* Vol. 27, No. 4, 1986, pp. 29–35.

[7]Panda, B., and Chopra, I., "Dynamics of Composite Rotor Blades in Forward Flight," *Vertica,* Vol. 11, No. 1/2, 1987, pp. 187–209.

[8]Bauchau, O. A., "A Beam Theory for Anisotropic Materials," *Journal of Applied Mechanics,* Vol. 52, June 1985, pp. 416–422.

[9]Bauchau, O. A., and Hong, C. H., "Large Displacement Analysis of Naturally Curved and Twisted Composite Beams," *AIAA Journal,* Vol. 25, No. 11, 1987, pp. 1469–1475.

[10]Bauchau, O. A., and Hong, C. H., "Nonlinear Composite Beam Theory," *Journal of Applied Mechanics,* Vol. 55, March 1988, pp. 156–163.

[11]Stemple, A. D., and Lee, S. W., "Finite Element Model for Composite Beams with Arbitrary Cross-Sectional Warping," *AIAA Journal,* Vol. 26, No. 12, 1988, pp. 1512–1520.

[12]Rand, O., "Theoretical Modelling of Composite Rotating Beams," *Vertica,* Vol. 14, No. 3, 1991, pp. 329–343.

[13]Nixon, M. W., "Extension-Twist Coupling of Composite Circular Tubes with Application to Tilt Rotor Blade Design," AIAA 28th Structures, Structural Dynamics and Materials Conference, 1987.

[14]Srinivasnan, A. V., Cutts, D. G., Shu, H. T., Sharpe, D. L., and Bauchau, O. A., "Structural Dynamics of a Helicopter Rotor Blade System," *Journal of the American Helicopter Society,* Vol. 35, No. 1, 1990, pp. 75–85.

[15]Chandra, R., and Chopra, I., "Dynamic Testing of Thin-Walled Composite Box Beams in a Vacuum Chamber," *Proceedings of the AHS National Specialist's Meeting on Rotorcraft Dynamics,* Arlington, TX, Nov. 1989.